Design, Synthesis, and Biological Characterization of a Caspase 3/7 Selective Isatin Labeled with 2-[^{18}F]fluoroethylazide

Graham Smith,[†] Matthias Glaser,[‡] Meg Perumal,[†] Quang-De Nguyen,[†] Bo Shan,[‡] Erik Årstad,[‡] and Eric O. Aboagye*[,†]

Molecular Therapy Group, Faculty of Medicine, Imperial College London, Hammersmith Hospital, Du Cane Road, London W12 0NN, United Kingdom, MDx Discovery (part of GE Healthcare) at Hammersmith Imanet Ltd, Hammersmith Hospital, Du Cane Road, London W12 0NN, United Kingdom

Received June 26, 2008

Imaging of programmed cell death (apoptosis) is important in the assessment of therapeutic response in oncology and for diagnosis in cardiac and neurodegenerative disorders. The executioner caspases 3 and 7 ultimately effect cellular death, thus providing selective molecular targets for in vivo quantification of apoptosis. To realize this potential, we aimed to develop ^{18}F-labeled isatin sulfonamides with high metabolic stability and moderate lipophilicity while retaining selectivity and affinity for caspase 3/7. A small library of isatins modified with fluorinated aromatic groups and heterocycles was synthesized. A lead compound incorporating 2′-fluoroethyl-1,2,3-triazole was identified with subnanomolar affinity for caspase 3. "Click labeling" provided the ^{18}F-labeled tracer in 65 ± 6% decay-corrected radiochemical yield from 2-[^{18}F]fluoroethylazide. The compound showed high stability in vivo with rapid uptake and elimination in healthy tissues and tumor. The novel ^{18}F-labeled isatin is a candidate radiotracer for further preclinical evaluation for imaging of apoptosis.

Introduction

Apoptosis or programmed cell death (PCD) is the most prevalent cell death pathway and proceeds via a highly regulated, energy conserved mechanism.[1] In the healthy state, apoptosis plays a pivotal role in controlling cell growth. Dysregulation of this process has been implicated in a number of disease states such as cancer, autoimmunity, neurodegeneration, ischemia, and transplant rejection.[2,3] Noninvasive imaging of apoptosis will therefore be of immense value for early assessment of response to therapeutic intervention and can provide new insight into devastating pathological processes. Early monitoring of the efficacy of cancer therapy is of particular interest. Apoptosis is regulated by both intrinsic (via mitochondria) and extrinsic (activation of death receptors) signaling networks that control a family of enzymes known as caspases (cysteine aspartate specific proteases).[4,5] The pathways activate "initiator" caspases 8 (extrinsic) or 9 (intrinsic), which in turn cleave the inactive pro-caspases 3, 6, and 7 into the active "executioner" caspases 3, 6, and 7.[1] The executioner caspases ultimately effect cellular death through cleavage of cellular proteins, which occurs adjacent to aspartate residues in a highly selective manner. The proteins cleaved include DNA repair enzymes (e.g., PARP[a]), key signaling proteins (e.g., Akt, Ras), nuclear skeletal proteins (e.g., actin, fodrin, lamins), and cell cycle regulators (e.g., p27Kip1).[6]

Following a high throughput screen, Lee and co-workers identified the isatin **1** as an inhibitor of caspase 3 (Chart 1).[7] Structural optimization led to the discovery of the highly potent sulfonamide **2** (2.5 nM). Realizing the potential of radiolabeled isatins for imaging of apoptosis, the groups of Kopka and Mach independently developed the ^{18}F-labeled fluoroethyl phenyl ether **3** as a putative tracer for positron emission tomography (PET) imaging of activated caspase 3 levels.[8,9] Recently, Mach and co-workers reported that the uptake of [^{18}F]**3** increases in the liver and spleen of rats treated with cycloheximide, a model for chemically induced apoptosis.[10] To further characterize this class of compounds, we investigated the biological properties of a radioiodinated analogue [^{125}I]**4**.[9] The results indicated poor biological stability and led us to design a new series of isatins. Here we report the development and characterization of a novel ^{18}F-labeled isatin with improved metabolic profile, reduced lipophilicity, and subnanomolar affinity for capsase 3.

Results

Chemistry. The isatins **2**, **4**, and **5** were synthesized as described in the literature.[7–9] Compound **6** was obtained by alkylation of 5-[1-(pyrrolidinyl)sulfonyl]isatin[7] with 4-fluorobenzyl bromide. The isatin **5** was chosen as lead compound, and modifications were made to the left side ether moiety and at the N-1 position with the aim to improve the biological stability while retaining selectivity and affinity for caspase 3. To achieve this, we incorporated fluorine groups into the left side phenyl ether group and also investigated the tolerance of heterocycles in this position. Of particular interest was the tolerance to 1,2,3-triazoles, as this group is reportedly inert to metabolic degradation[11,12] and can be readily labeled with fluorine-18.[12–14] The target compounds were synthesized by condensation of functionalized pyrrolidines with 5-chlorosulfonylisatin and subsequent alkylation of the isatin nitrogen using potassium carbonate/DMF (Scheme 1).

* To whom correspondence should be addressed. Phone: +44-208-383-3759. Fax: +44-208-383-1783. E-mail: eric.aboagye@imperial.ac.uk.

[†] Molecular Therapy Group, Faculty of Medicine, Imperial College London, Hammersmith Hospital.

[‡] MDx Discovery (part of GE Healthcare) at Hammersmith Imanet Ltd, Hammersmith Hospital.

[a] Abbreviations: PARP, poly (ADP-ribose) polymerase; DMF, *N*,*N*-dimethylformamide; BOC, *tert*-butoxycarbonyl; DIAD, diisopropyl azodicarboxylate; DCM, dichloromethane; TFA, trifluoroacetic acid; TEA, triethylamine; THF, tetrahydrofuran; CDDP, *cis*-dichlorodiammine platinum(II); RIPA, radio-immunoprecipation assay; SDS, sodium dodecyl sulfate; PVDF, polyvinylidene fluoride; HRP, horseradish peroxidase; DMSO, dimethyl sulfoxide; CCPMA, corrected counts per minute average; CHAPS, 3-[(3-cholamidopropyl)dimethylammonio]-1-propanesulfonic acid; HEPES, 4-(2-hydroxyethyl)piperazine-1-ethanesulfonic acid; EDTA, ethylenediamminetetraacetic acid; BCA, bicinchoninic acid.

10.1021/jm801107u CCC: $40.75
Published on Web 12/02/2008

Chart 1

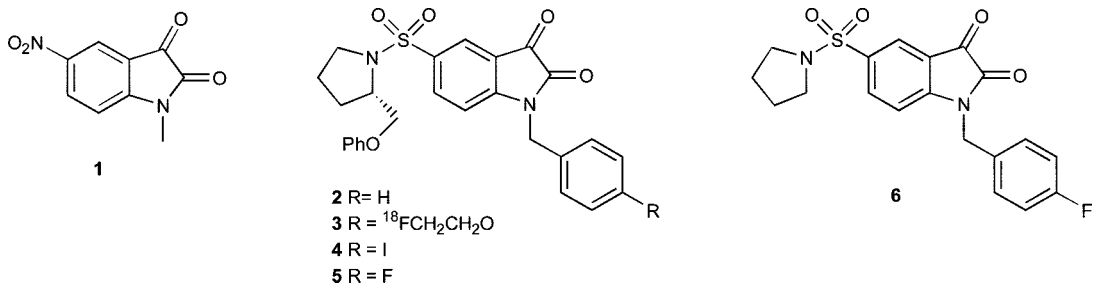

Scheme 1[a]

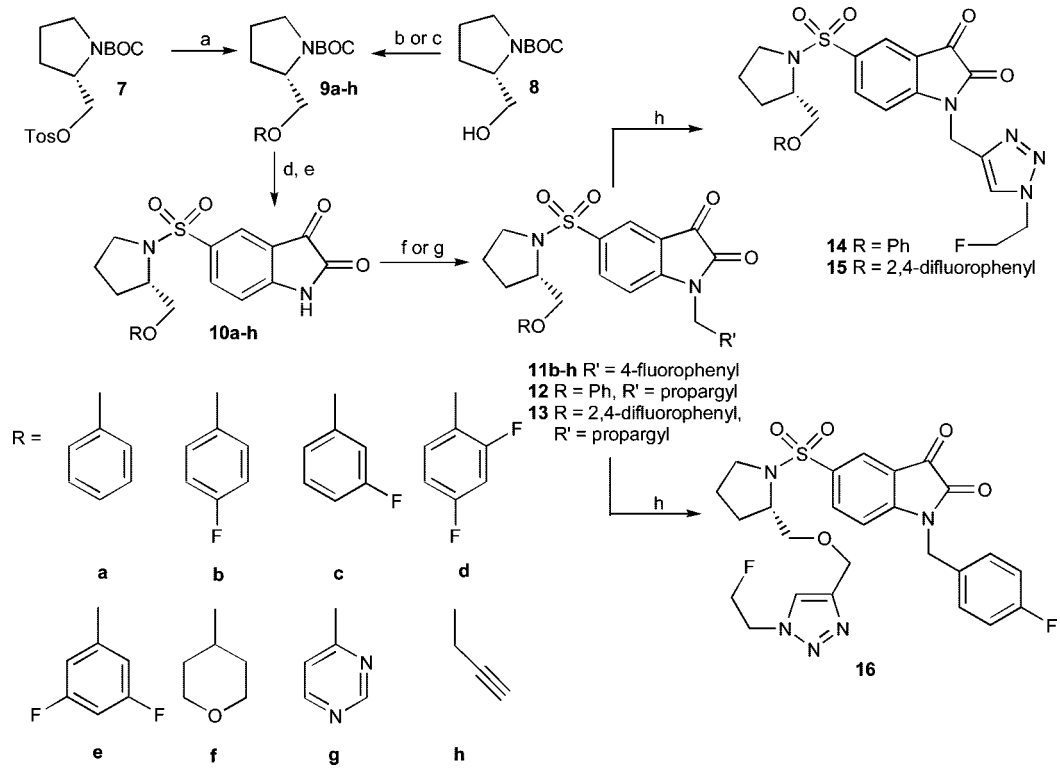

[a] Reagents and conditions: (a) phenol/fluoro-substituted phenol/4-tetrahydropyran, NaH, DMF, 80°C, 17 h; (b) 4(3*H*)-pyrimidone, PPh_3, DIAD, DCM, rt, 48 h; (c) propargyl bromide, KOH, DMF, rt, 18 h; (d) TFA, DCM, 0°C, 1 h; (e) 5-chlorosulfonylisatin, TEA, THF/DCM, rt, 19 h; (f) 4-fluorobenzyl bromide, K_2CO_3, DMF, rt, 2 h; (g) propargyl bromide, K_2CO_3, DMF, rt, 2 h; (h) 2-fluoroethyl azide, $CuSO_4$, L-ascorbic acid, DMF, rt, 2 h.

Reaction of commercially available phenols as well as 4-hydroxytetrahydropyran with tosylate **7** provided the pyrrolidines **9a**−**f** in good yield. 4(3*H*)-Pyrimidone was coupled with the alcohol **8** using a modification of the procedure reported by Wipf et al.[15] to furnish the pyrrolidine **9g** in 69% yield. O-Alkylation of **8** with propargyl bromide afforded the corresponding ether **9h** in 67% yield. Deprotection of the BOC protected pyrrolidines **9a**−**h** with trifluoroacetic acid followed by conjugation with 5-chlorosulfonylisatin provided the sulfonamides **10a**−**h** in moderate to good yields. Subsequent treatment of **10b**−**h** with 4-fluorobenzyl bromide under basic conditions yielded the target compounds **11b**−**h**, whereas treatment of **10a** and **10d** with propargyl bromide provided the alkynes **12** and **13**, respectively. The triazoles **14**−**16** were prepared by copper catalyzed cycloaddition of 2-fluoroethylazide with the respective alkyne precursors **11h**, **12**, and **13**. Somewhat surprisingly, the isatin scaffold decomposed on heating at 90 °C in the presence of the copper sulfate and ascorbic acid, resulting in poor yields of the target triazoles **14**−**16**. The issue was partly resolved by increasing the copper sulfate concentration from 5% to 50% relative to the alkyne precursor, carrying out the reaction at ambient temperature and reducing the reaction time to 1 h, which provided the triazoles **14**−**16** in yields of 48−57%.

Radiochemistry. The triazole **15** was labeled by copper catalyzed cycloaddition of 2-[^{18}F]fluoroethylazide ([^{18}F]**17**) with the alkyne precursor **13**. [^{18}F]**17** was prepared by reaction of [^{18}F]fluoride with the corresponding tosylate precursor **18** and was purified by distillation as previously described (Scheme 2).[14]

Investigation of the impact of the catalytic system, temperature, and pH on the radiochemical yield revealed poor thermal stability of [^{18}F]**15**, with the highest yields obtained at room temperature. Addition of sodium phosphate buffer (pH 6.0, 250 mM)) to the reaction mixture dramatically improved the radiochemical yield, whereas only minor differences were observed for the two catalytic systems investigated (copper powder or copper sulfate/ascorbate). The optimal conditions were found to be 30 min reaction time at room temperature in the presence of a slight excess of copper sulfate relative to the alkyne precursor **13**. This provided the triazole [^{18}F]**15** in 65 ± 6% (n = 26, decay-corrected from [^{18}F]**17**) isolated radiochemical yield with a radiochemical purity of >99% after purification

Scheme 2[a]

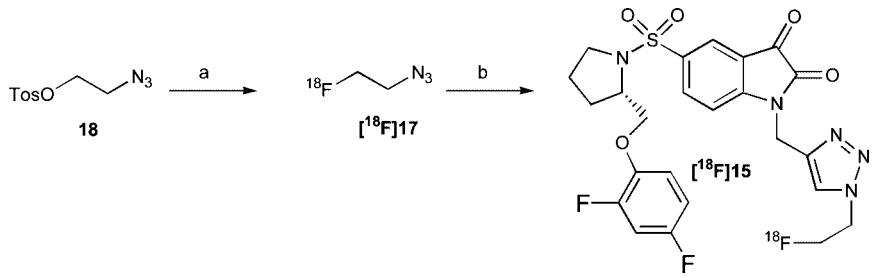

[a] Reagents: (a) [18F]KF, Kryptofix[2,2,2], K_2CO_3, acetonitrile, 80°C, 15 min; (b) $CuSO_4$, sodium ascorbate, phosphate buffer pH 6.0, rt, 30 min, **13**.

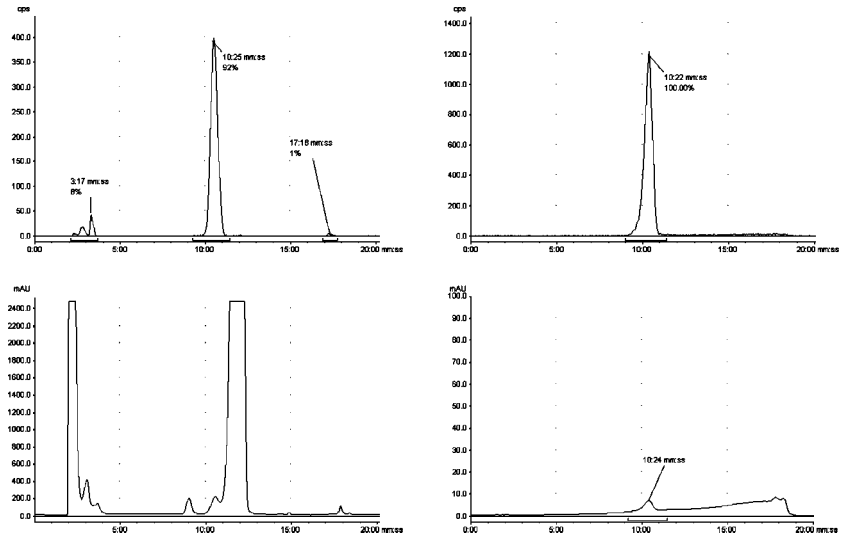

Figure 1. Typical preparative HPLC trace of reaction mixture containing [18F]**15** (left) and corresponding trace after formulation of [18F]**15** (right) (top: radioactivity channel; bottom: UV channel at 254 nm).

by HPLC. A typical HPLC chromatogram for the product mixture is shown in Figure 1. As the procedure was carried out manually with low amounts of radioactivity, only modest specific activity (1.2 GBq/μmol) was achieved at end of synthesis. The identity of [18F]**15** was confirmed by coelution with the nonradioactive reference compound. The purified [18F]**15** was formulated by solid-phase extraction with an efficiency of 91 ± 6% (n = 26, decay-corrected). The radiosynthesis including formulation of [18F]**15** took three hours in total.

Enzyme Assays. The affinities of the novel fluorinated isatins **11b**−**h** and **14**−**16** for different activated caspases 1, 3, 6, 7, and 8 were measured by a fluorimetric in vitro caspase inhibition assay similar to that described by Kopka and co-workers.[9] Inhibition of recombinant human caspases was assessed by measuring the accumulation of a fluorogenic product, 7-amino-4-methylcoumarin (7-AMC). Compounds **2** and **4**−**6** were included as reference compounds. The results are summarized in Table 1. The data are the average for two runs, each done in duplicate, at 9 concentrations ranging from 5 pM to 500 μM; the drug concentration required to inhibit each enzyme by 50% (EC_{50}) was obtained from nonlinear regression analysis of the inhibition profiles. In this assay, the affinity of the iodinated isatin **4** was 59.9 and 25.3 nM for caspase 3 and 7, respectively. Substituting the iodine for fluorine as in compound **5** led to a slight increase in affinity for both caspase 3 and 7. The importance of the left side ether group was clearly demonstrated by analysis of isatin **6**, which with 199.5 nM affinity for caspase 3 was 4-fold less potent than isatins **4** and **5**. Fluorine substituents on the phenyl ether were well tolerated and, for the isatins **11b**−**c**, the affinity for caspase 3 increased 2-fold as compared with nonfluorinated phenyl ether **4**. The difluorinated isatins **11d**−**e** were even more potent, with an affinity of 12.4 and 10.4 nM for caspase 3, respectively. Similar affinities were found for the tetrahydropyran **11f**, and replacement of the phenyl ether with a pyrimidinyl group as in **11g** led to a further increase in potency, with affinities of 5.5 and 2.3 nM for caspase 3 and 7, respectively. Gratifyingly, introduction of 2′-fluoroethyl-1,2,3-triazole on either side of the molecule led to a sharp increase in potency, with measured caspase 3 affinities of 16.7 and 12.6 nM for the triazoles **14** and **16**, respectively. Of the compounds tested, the triazole **15** was by far the most potent, with affinities of 0.5 and 2.5 nM for caspase 3 and 7, respectively. All the compounds tested were poor substrates for caspases 1, 6, and 8 (EC_{50} > 5000 nM).

Biodistribution and Metabolic Stability. Radioiodination of isatin **4** afforded the opportunity for facile and rapid assessment of the suitability of this compound class as apoptosis imaging agents. To achieve this, isatin **4** was radiolabeled with iodine-125 ($t_{1/2}$ = 59.9 days) by iodo-destannylation using the method of Kopka.[9] The radiotracer [125I]**4** was injected intravenously into mice, and its tissue distribution was measured in the major organs at selected time points from 2 to 60 min after injection. The radiotracer distributed rapidly to the major organs and was also rapidly eliminated (Figure 2). The in vivo stability of [125I]**4** in mice was determined in plasma and liver at selected time points from 2 to 60 min after tracer injection. The radiotracer [125I]**4** was completely eliminated from plasma within 10 min and represented <15% (n = 3) of the radioactivity detected in the liver at this point of time (chromatograms

Table 1. Caspase Inhibition Profile for Selected Compounds

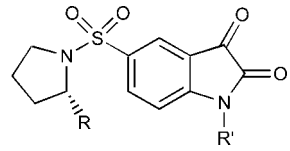

	R	R′	caspase EC_{50} (nM)[a]			cLog P[b]
			3	7	1/6/8	
2	phenoxymethyl	benzyl	41.8	29.4	>5000	3.65
4	phenoxymethyl	4-iodobenzyl	59.9	25.3	>5000	4.68
5	phenoxymethyl	4-fluorobenzyl	50.5	19.8	>5000	3.70
6	H	4-fluorobenzyl	199.5	78.6	>5000	1.93
11b	4-fluorophenoxymethyl	4-fluorobenzyl	26.1	8.0	>5000	3.83
11c	3-fluorophenoxymethyl	4-fluorobenzyl	17.0	13.5	>5000	3.80
11d	2,4-difluorophenoxymethyl	4-fluorobenzyl	12.4	13.0	>5000	3.87
11e	3,5- difluorophenoxymethyl	4-fluorobenzyl	10.4	16.8	>5000	3.94
11f	4-tetrahydropyranyloxymethyl	4-fluorobenzyl	10.7	14.4	>5000	1.87
11g	pyrimidin-4-yloxymethyl	4-fluorobenzyl	5.5	2.3	>5000	2.06
13	2,4-difluorophenoxymethyl	2-propynyl	50.1	60.4	>5000	2.42
14	phenoxymethyl	1-(2-fluoroethyl)-1*H*-[1,2,3]-triazol-4-ylmethyl	16.7	28.2	>5000	1.38
15	2,4-difluorophenoxymethyl	1-(2-fluoroethyl)-1*H*-[1,2,3]-triazol-4-ylmethyl	0.5	2.2	>5000	1.55[c]
16	1-(2-fluoroethyl)-1*H*-[1,2,3]-triazol-4-ylmethoxymethyl	4-fluorobenzyl	12.6	18.3	>5000	1.55

[a] Each value is an average of two independent measurements each obtained from a fit to a 9-concentration level data set ($r^2 > 0.9$). [b] Values calculated using ACD/Chemsketch Laboratories 10.02. [c] Measured Log $P = 1.61$.

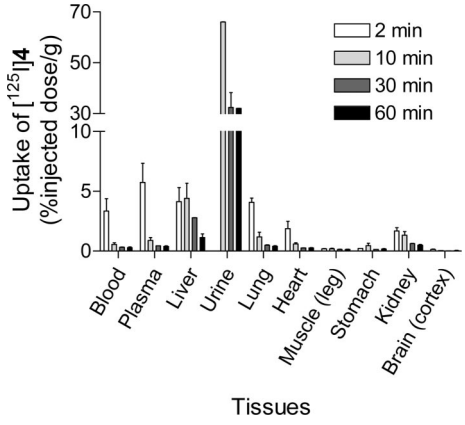

Figure 2. Tissue distribution of [^{125}I]**4** in untreated nontumor bearing mice at 2, 10, 30, and 60 min. Data are mean ± SEM; $n = 3$ mice per time point. There was no 2 min urine sample.

supplied in Supporting Information). Within 30 min after injection, the parent [^{125}I]**4** was fully metabolized in the liver, with a single, polar metabolite constituting the majority of the radioactivity detected. Consistent with these findings, we observed rapid clearance in all tissues investigated, and from 10 min onward, the majority of the injected radioactivity was excreted in the urine (Figure 2).

Organ distribution studies pointed to a metabolic pathway other than deiodination, as radioactivity in the stomach, which is known to accumulate radioiodide, was low. To identify the main site of metabolism, we compared the metabolic fate of compounds **4**[7] and **5**[8] (Chart 1) to that of **6** after in vitro incubation with murine liver S9 fraction. As shown in Figure 3, the metabolic profiles of isatins **4** and **5** were similar, with near complete degradation observed after 60 min incubation. In contrast, the isatin **6** was markedly more stable and remained largely intact at this time. While no attempts were made to identify the nature of the metabolites, the results indicate that the isatin scaffold is relatively stable, whereas the phenyl ether group in **4** and **5** undergoes rapid breakdown consistent with aromatic hydroxylation.

It is well-known that the introduction of fluorine to aromatic groups not only blocks P450-catalyzed ring hydroxylation of the substituted carbon but also reduces metabolic attack on neighboring nonsubstituted carbons by exerting a strong electron withdrawing effect.[16,17] If aromatic hydroxylation indeed is the major metabolic pathway for degradation of the isatins investigated, the 2,4-difluorophenyl ether containing **15**, the most potent compound in the enzyme assay, should be significantly more stable in vivo compared to unsubstituted phenyl ethers (e.g., **4**). We tested this hypothesis, first by assessing the behavior of **15** and [^{18}F]**15** in cell-based assays and then by analyzing the stability of [^{18}F]**15** over time in mice.

We assessed the cellular activity of the most active compound in the enzyme assay (isatin **15**) against the previously analyzed[9] iodo compound **4**. Figure 4 shows that preincubation of RIF-1 cells with isatin **15**, but not **4**, disrupted the induction of caspase 3 cognate target PARP by cisplatin (CDDP), demonstrating cellular activity of **15**. To further establish the binding of istain **15** under conditions of drug-induced apoptosis, we then evaluated uptake of radiolabeled [^{18}F]**15** in RIF-1 cells. The results are summarized in Figure 5 and show a statistically significant increase in uptake of [^{18}F]**15** of 1.5-fold for treated compared to untreated cells ($p = 0.04$).

Following the findings of the cellular assays using **15** and [^{18}F]**15**, the radiotracer [^{18}F]**15** was injected intravenously into tumor-bearing mice and its tissue distribution was measured in selected tissues at 2, 15, and 60 min after injection. Furthermore, the in vivo metabolic stability of the radiotracer was determined in plasma, liver, and urine samples. Figure 6 shows that [^{18}F]**15** distributed rapidly to tissues and was also rapidly eliminated. High localization of [^{18}F]**15**-derived radioactivity was seen in kidney, urine, and liver, suggesting the importance of both renal and hepatic routes of elimination. However, even in these tissues, rapid elimination of radioactivity was seen. Importantly, from an imaging standpoint, the rapid clearance of [^{18}F]**15** in untreated tumors and heart should facilitate measurement of increased binding associated with caspase activation in these tissues. Bone uptake was low, suggesting an absence of in vivo defluorination and hence metabolic stability of the 2′-fluoroethyl-1,2-3-triazole moiety. Tumor uptake studies were also carried out in control and CDDP treated RIF-1 tumor bearing mice (24 h after treatment) to assess the effect of CDDP treatment on [^{18}F]**15** tumor uptake in vivo. Figure 7 shows an increase in [^{18}F]15-derived radioactivity by 2.9-fold in CDDP treated

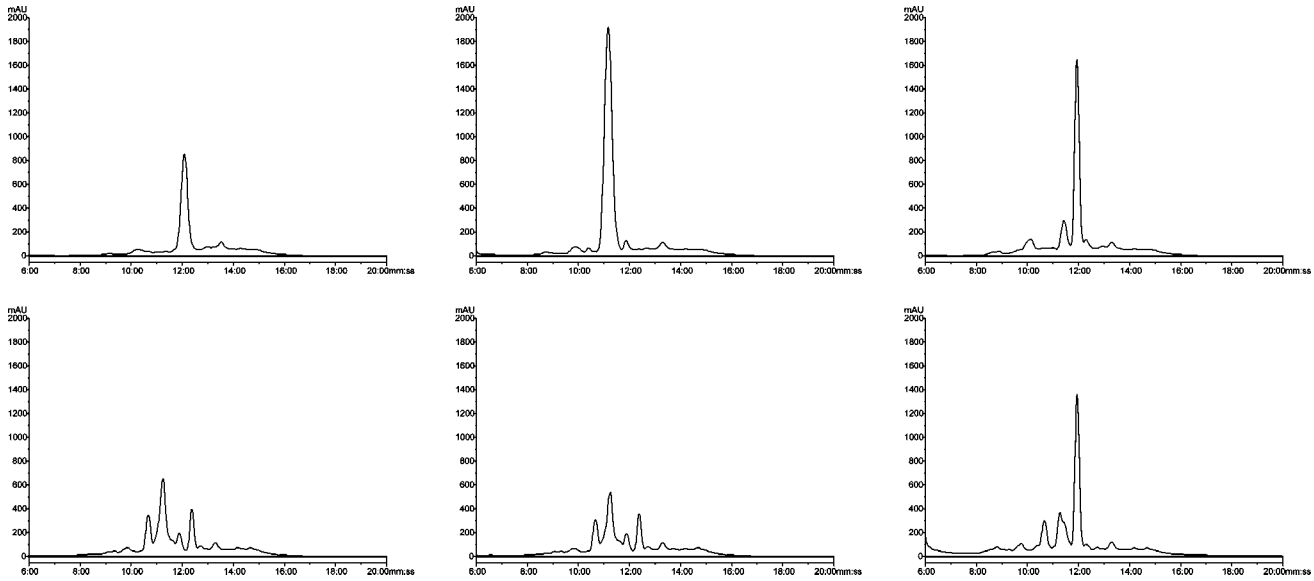

Figure 3. Representative HPLC profiles of isatins incubated with mouse liver S9 fractions. Upper row shows, from left to right, isatin **4**, **5**, and **6** as they appear at zero time. Lower row shows, from left to right, isatin **4**, **5**, and **6** after incubation for 60 min.

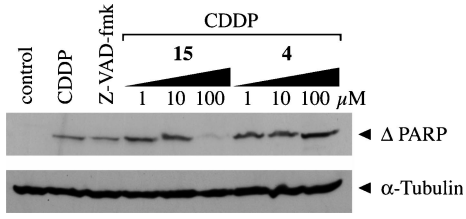

Figure 4. Cellular activity of isatin **15** and **4** assessed by Western blot analysis. Inhibitory activity of isatin **15** and **4** on the caspase 3 cognate target PARP. RIF-1 cells were treated for 15 min with the caspase inhibitors Z-VAD-FMK (100 μM), isatin **15** and **4**, prior to apoptosis induction with CDDP (100 μM) for 48 h. The Δ PARP immunoblot band corresponds to the endogenous 89 kDa large fragment of PARP resulting from caspase 3 cleavage. α tubulin was used as a loading control.

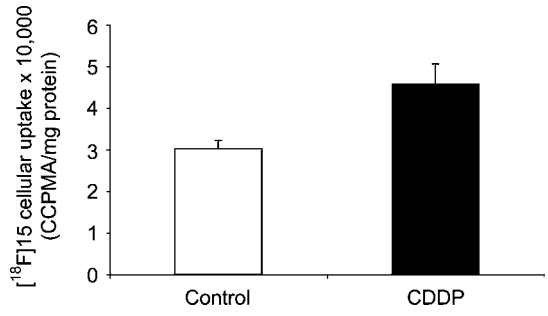

Figure 5. Uptake profile of [^{18}F]**15** in RIF-1 cells treated with vehicle or CDDP. RIF-1 cells were treated with vehicle (0.1% DMSO) or CDDP (100 μM) for 48 h. The cells were then incubated with [^{18}F]**15** for 1 h, washed and analyzed for radioactivity. Data are expressed as decay-corrected counts per min averaged per milligram of total cellular protein. Data are mean ± SEM done in triplicate.

compared to control tumor, suggesting that [^{18}F]**15** is promising enough to warrant further evaluation as an in vivo caspase-3/7 imaging agent.

In keeping with our design goals, radio-HPLC analysis showed that [^{18}F]**15** was relatively more stable to metabolic degradation (Figure 8), producing a single polar metabolite peak in plasma and liver. The parent compound was still present in plasma at 60 min and was the dominant peak. In contrast, the metabolite was the dominant peak in liver samples at all time

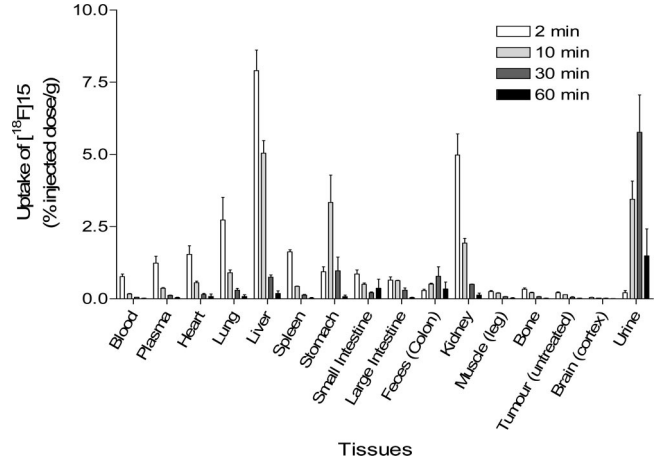

Figure 6. Biodistribution of [^{18}F]**15** in RIF-1 tumor bearing mice between 2 and 60 min. Data are mean ± SEM; $n = 3-6$ mice per time point.

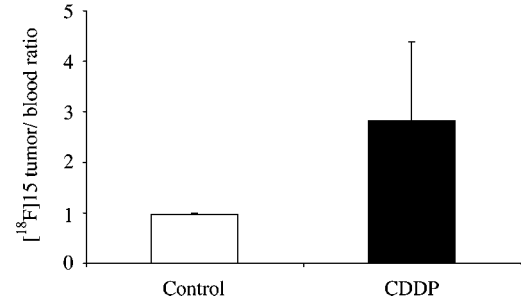

Figure 7. Uptake of [^{18}F]**15** in RIF-1 tumor treated with vehicle (control: 50% DMSO) or CDDP (10 mg/kg single dose). The [^{18}F]-derived radioactivity levels at 60 min post radiotracer injection were analyzed and expressed as a ratio to that of blood. Data are mean ± SEM and $n = 8$ mice per group.

points studied. Urine radioactivity comprised mainly of the metabolite (traces provided in supplementary section). The proportions of parent radiotracer in plasma and liver at the selected time points, together with the apparent extraction efficiency are summarized in Table 2. Following a rapid decrease, the rate of in vivo metabolism appeared to plateau

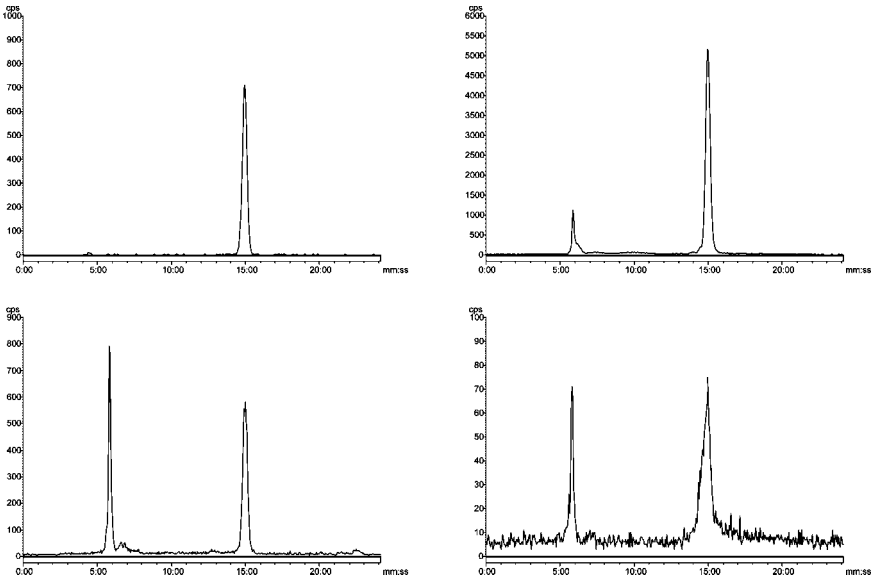

Figure 8. In vivo metabolism of [^{18}F]**15** assessed in plasma by radio-HPLC. Top left, [^{18}F]**15** standard; top right, 2 min plasma; bottom left, 15 min plasma; bottom right, 60 min plasma.

Table 2. In Vivo Metabolism of [^{18}F]**15** at Selected Time Points Showing the Proportion of [^{18}F]**15** Present in Plasma and Liver Extracts[a]

time (min)	parent (plasma)[b]	recovery (plasma)[b]	parent (liver)[c]	recovery (liver)[c]
2	86.1 ± 3.7	92.1 ± 3.4	35.7/43.4	79.7/86.9
15	61.3 ± 5.9	76.8 ± 5.2	9.7/10.2	67.1/68.9
60	64.8 ± 7.0	50.9 ± 3.7	27.0/29.7	46.4/65.2

[a] The extracts were analyzed by radio-HPLC. The efficiencies of extraction of radioactive analytes from the samples are reported below. [b] Average of 3 independent studies per time point. [c] Individual results from independent studies. Individual results from two samples are reported for liver. Proportion [^{18}F]**15** in plasma and liver were calculated by comparison of [^{18}F]**15** peak to total radioactivity present on chromatogram; recovery was calculated by comparing the amount of radioactivity extracted from the tissue sample to the radioactivity in an equivalent volume of tissue plasma or homogenate.

between 15 and 60 min. There was also a time-dependent increase in radioactivity in the residual pellets after plasma extraction, suggesting an increase in binding to plasma proteins. We do not know if this is due to nonspecific binding or related to binding of the isatin to a specific recognition site on plasma proteins.

Discussion

We have developed a high affinity and metabolically stable 2-[^{18}F]fluoroethylazide-conjugated isatin sulfonamide for use in studying caspase 3/7 activation and apoptosis in vivo. The isatin [^{18}F]**15** meets several of the design goals of a good imaging agent, including subnanomolar affinity for caspase 3, high selectivity for target, potential for efficient radiolabeling to generate high specific radioactivity product, moderate lipophilicity, and high metabolic stability. Apoptosis is one of the major mechanisms of cell death and hence an important target for imaging therapeutic response in cancer. Beyond cancer, it has a role in the evaluation of pathophysiology of neurodegeneration, acute myocardial infarction, and chronic heart failure. Of the probes available for imaging cell death, radiolabeled annexin V has received the most attention.[18,19] With regards to membrane interacting probes, a number of *N*,*N*-didansyl cysteine, dansyl ethylfluoroalanine, and malonic acid derivatives have also been developed to image apoptosis.[20–22]

More recently there has been a growing interest in the development of compounds that bind to activated executioner caspases as potential probes for studying caspase-dependent apoptosis, as these should be more specific than membrane activity for apoptosis. The suitability of imaging probes based on the caspase-3-specific DEVD (Asp-Glu-Gly-Asp) peptide sequence (optimum substrate sequence)[23] has been tested in one study.[24] The highly polar nature of the DEVD sequence, however, resulted in poor cellular uptake, making the peptide-based strategy less attractive for use in PET imaging. Further attachment of a Tat sequence resulted in increased caspase-3-independent unidirectional cellular uptake;[24] again this property made it unsuitable for imaging. The groups of Kopka and Mach have independently developed ^{18}F-labeled fluoroethyl phenyl ether isatins as putative tracers for imaging caspase activation by PET.[8,9] The mechanism of action of isatins involves formation of an intracellular enzyme−inhibitor complex with caspase 3 (and 7) through covalent binding to the enzyme active site of the activated caspase.[25,26] The dicarbonyl functionality of the isatin is essential to its mechanism of action; it binds to the cysteine residue of the active site, forming a thiohemiketal via the electrophilic C-3 carbonyl carbon of the isatin and the nucleophilic cysteine thiolate functionality.[26]

Our initial studies with [^{125}I]**4** suggested that structural optimization was necessary to develop novel radiotracers which are stable in vivo. Comparison of the metabolic profile of isatins **4**−**6** in a murine liver S9 in vitro assay pointed to the (*S*)-2-phenoxymethyl moiety as the major site of metabolism. This led us to design a focused library of isatins incorporating heterocycles and fluorine substituted aromatic groups in this position. Motivated by the need for efficient labeling chemistry, increased polarity, and metabolic stability, we incorporated 2′-fluoroethyl-1,2,3-triazole in the N-1 position as well as on the left side ether position of the isatin 5-sulfonamide scaffold. In total 10 novel compounds were synthesized and evaluated for caspase affinity. Introduction of fluorine to the (*S*)-2-phenoxymethyl moiety led to a 3-fold increase in caspase 3 affinity, with 3-substituted **11c** being slightly more potent than the 4-substituted **11b**. Addition of a second fluorine group was well tolerated with the 2,4 disubstituted **11d** and the 3,5 disubstituted **11e** being equipotent to **11c**. According to the molecular modeling studies reported by Chu and co-workers, the (*S*)-2-phenoxymethyl moiety interacts with the S_3 binding domain through $\pi-\pi$

binding with Phe381.[8] The improved affinity of the fluorinated derivatives could be due to more favorable π stacking or hydrogen bonding with other groups in the S_3 domain such as Ser381.[27] The 6-fold increase in potency of the tetrahydropyran **11f** as compared to the (*S*)-2-phenoxymethyl **5** is surprising given that this ring is fully saturated, however, according to the model of Chu, the oxygen atom in the tetrahydropyran moiety would be expected to form a strong hydrogen bond with the hydroxyl group of Ser381.[8] The pyrimidyl derivative **11g** should benefit from both favorable $\pi-\pi$ binding with Phe381 and hydrogen bonding with Ser381, which explains the high potency of this compound. The potency of the fluoroethyltriazole **16** was similar to that of the fluorinated aryl ether **11b−e**, which is surprising given the considerable smaller size and higher polarity of this group. Lee[7] denoted the binding domain around the isatin nitrogen as a hydrophilic pocket, and most groups have since included benzyl moieties in this position. It was therefore highly unexpected that the triazole **14** is 4-fold more potent than the benzyl derivative **5**, which suggests the presence of hydrophilic groups in this binding domain. Gratifyingly, combining the fluoroethyltriazole group on the isatin nitrogen with the 2,4-difluorinated aryl ether moiety to give **15** led to a sharp increase in caspase 3 affinity ($EC_{50} = 0.5$ nM). Analysis of the cellular inhibition profile indicates that **15** is more potent than **4**. This correlates with the findings in a previous study by Kopka et al.,[9] which also reported differences in the cellular caspase-3 inhibition profile for different isatin analogues. Isatin **15** has a cellular inhibitory potency in the 50−100 μM range, comparable to the most active compounds reported by Kopka et al.[9] The basis of this finding is not clearly understood. Furthermore, the increased uptake of [18F]**15** under conditions of drug induced apoptosis in cells and tumors supports the view that [18F]**15** warrants further evaluation as an in vivo apoptosis marker.

Our studies have highlighted the need to consider metabolic stability as well as labeling efficiency early in the discovery of probes. "Click labeling" of the isatin precursor **13** with 2-[18F]fluoroethylazide proceeded in high radiochemical yields, and the resulting triazole [8F]**15** demonstrated high metabolic stability, with no indication of defluorination in vivo. The modest specific activity (1.2 GBq/μmol) was a concern for us, given that [18F]**15** is acting as a binding molecule (as distinct from a substrate). However, our results indicated that the specific activity was sufficient for the initial evaluation of [18F]**15**. As we progress into more sophisticated in vivo models or clinical development, this issue will be fully addressed. The rapid clearance of [18F]**15** in the heart and untreated tumors is a clear advantage for imaging of caspase 3/7 activity in these tissues. The overall low values for uptake in untreated tumor in the biodistribution study (Figure 6) is likely the result of the low levels of apoptosis (approximately 1%) in the RIF-1 tumor model.[28] In contrast, the high localization of [18F]**15**-derived radioactivity in liver will preclude the use of liver models of apoptosis in the preclinical evaluation of this tracer, as results from such models will be difficult to interpret.[10]

Conclusion

We have designed, synthesized, and radiolabeled a novel isatin 5-sulfonamide that has potential utility for imaging caspase-dependent cell death. The approach described here involved design of a focused library of compounds based on metabolic stability, affinity, and ease of radiolabeling considerations. This strategy permitted isotopic radiolabeling of high affinity compounds discovered from screening such a library. The synthesis of a focused library of isatins led to identification of an 1,2,3-triazole conjugated compound with subnanomolar affinity for caspase-3. "Click labeling" with 2-[18F]fluoroethylazide proceeded in high radiochemical yields, and the resulting triazole demonstrated high metabolic stability, with no indication of defluorination in vivo. The rapid clearance of the 18F-labeled isatin from heart and untreated tumor suggests that the compound is suitable for imaging of apoptosis in these tissues.

Experimental Section

Chemistry. Reagents and solvents were purchased from Sigma-Aldrich (Gillingham, United Kingdom) and used without further purification. Potassium hydroxide and potassium carbonate were stored in a vacuum desiccator over phosphorus pentoxide. All reactions were carried out under argon unless otherwise stated. Petroleum ether refers to the fraction that is distilled between 40 and 60 °C. Automated flash chromatography was performed on a CombiFlash Companion machine (Companion Presearch Ltd.), using RediSep 4 or 12 g normal phase silica cartridges (flow rate 12 or 26 mL/min). Manual flash chromatography was carried out using Davisil neutral silica (60 Å, 60−200 μm, Fisher Scientific, Loughborough, UK), solvent mixtures are quoted as volume/volume. ^{1}H NMR spectra were obtained on a Bruker Avance 600 MHz NMR machine and spectra are referenced to residual solvent. Coupling constants (*J*) are given in Hertz (Hz). GC-MS data was acquired under electron ionization using an Agilent 6890N system. Mass spectra were obtained in positive electrospray ionization mode on a WatersMicromass LCT Premier or a Finnigan MAT 900 XLT machine. Melting points were determined in capillary tubes on a Stuart Scientific SMP1 melting point apparatus and are uncorrected. Solvent mixtures for thin layer chromatography (TLC) are quoted as volume/volume and samples were developed on aluminum backed neutral silica plates (0.2 mm thickness) (Fluka, Seelze, Germany). Purity analysis for compounds **2**, **4**, **5**, **6**, **10b−10h**, **11b−11h**, **12**, **13**, **14**, **15**, and **16** was evaluated by analytical HPLC; compounds **9b−9h** were analyzed by GC-MS with only a single peak observed in the GC trace. Tabulated values of purity can be found in the Supporting Information, and the purity of all compounds was greater than 95%. [18F]Fluoride was produced by a cyclotron (GE PETrace) using the $^{18}O(p,n)^{18}F$ nuclear reaction with 16.4 MeV proton irradiation of an enriched $[^{18}O]H_2O$ target.

HPLC Methods. (a) Purity analysis of nonradioactive compounds was carried out on an Agilent 1100 series system with Laura 3 software (Lablogic, Sheffield, UK) with a Phenomenex Luna 50 mm × 4.6 mm (3 μm) HPLC column attached and a mobile phase of 0.1 M ammonium formate and methanol/acetonitrile (1.8:1 v/v), gradient (50% organic for 1 min; 50 → 90% organic in 14 min; 90% organic for 4 min; 90 → 50% organic phase for 4 min) flow rate 1 mL/min, and wavelength 254 nm.

(b) Preparative radio-HPLC was carried out on a Beckman System Gold equipped with a Bioscan Flowcount FC-3400 PIN diode detector (Lablogic) and a linear UV-200 detector (wavelength 254 nm). A Phenomenex Onyx C_{18} 100 mm × 10 mm HPLC column and a mobile phase of water and methanol/acetonitrile (1.8:1 v/v), gradient 45 → 90% organic in 20 min, and flow rate 3 mL/min.

(c) Analytical radio-HPLC was carried out as above but using a Bioscan Flowcount FC3200 sodium iodide/PMT gamma detector (Lablogic), a linear UV-200 detector (wavelength 254 nm), and a Phenomenex Luna 50 mm × 4.6 mm (3 μm) column with a mobile phase of water and methanol/acetonitrile (1.8:1 v/v), gradient 60 → 90% organic in 20 min, flow rate 1 mL/min.

Synthesis. The following compounds were synthesized according to established literature procedures and ^{1}H NMR spectral data was consistent with reported values: (*S*)-1-benzyl-5-(2-phenoxymethyl-pyrrolidine-1-sulfonyl)isatin **2**, (*S*)-1-(4-iodobenzyl)-5-(2-phenoxymethyl-pyrrolidine-1-sulfonyl)isatin **4**, and (*S*)-1-(4-fluorobenzyl)-5-(2-phenoxymethyl-pyrrolidine-1-sulfonyl)isatin **5**.

The radiotracer [^{125}I]**4** was synthesized using the method of Kopka[9] by GE Healthcare Ltd. (Little Chalfont, Buckinghamshire, UK) and supplied as a solution in ethanol (~37 MBq/mL) with 91.9% radiochemical purity and specific activity of approximately 2000 Ci/mmol.

1-(4-Fluorobenzyl)-5-(pyrrolidine-1-sulfonyl)isatin (6). To an ice-cold, stirred solution of 5-pyrrolidine-1-sulfonylisatin[7] (0.14 g, 0.5 mmol) in dry DMF (8 mL) was added sodium hydride (40 mg, 1 mmol). After 30 min, 4-fluorobenzyl bromide (0.38 g, 2 mmol) was added and the mixture allowed warm to room temperature. After 19 h, the orange solution was poured onto 10% aq NH_4Cl (25 mL) and extracted with DCM (3 × 15 mL). Following concentration in vacuo, the residue taken up in diethyl ether (10 mL) and washed with water (3 × 10 mL) and dried over Na_2SO_4. Chromatography (diethyl ether/hexanes) afforded the title compound as an orange gum (83 mg, 43%). HRMS (ESI) = 389.0988 $(M + H)^+$. Calcd for $C_{19}H_{18}FN_2O_4S$ 389.0971. ^{1}H NMR (600 MHz, $CDCl_3$) δ 8.05 (d, J = 1.5 Hz, 1H), 7.99 (dd, J = 8.4 Hz, J = 1.5 Hz, 1 H), 7.35−7.32 (m, 2 H), 7.09−7.06 (m, 2 H), 6.91 (d, J = 8.4 Hz, 1 H), 4.94 (s, 2 H), 3.25−3.23 (4 H, m), 1.84−1.79 (4 H, m). TLC (UV_{254}) R_f = 0.63 (4:1 ethyl acetate/hexanes). HPLC t_R = 6.83 min.

(*S*)-*tert*-Butyl 2-(4-Fluorophenoxymethyl)pyrrolidine-1-carboxylate (9b). To a stirred solution of 4-fluorophenol (0.27 g, 2.4 mmol) in dry DMF (10 mL) was added sodium hydride (60% w/w in mineral oil) (0.11 g, 2.8 mmol). After 30 min, ((*S*)-1-(*tert*-butoxycarbonyl)pyrrolidin-2-yl)toluene-4-sulfonate **7**[7] (0.71 g, 2.0 mmol) in dry DMF (5 mL) was then added and the mixture heated to 80 °C for 17 h. The reaction was allowed to cool to room temperature and poured over 1 M NaOH (25 mL) and extracted with DCM (3 × 15 mL). The combined organic fractions were reduced under vacuum and diethyl ether (20 mL) added and then washed with 1 M NaOH (1 × 20 mL), water (1 × 20 mL), and then brine (1 × 20 mL) and dried over Na_2SO_4. Chromatography (hexanes/ethyl acetate) gave the product as a colorless oil (0.36 g, 61%). HRMS (ESI) = 296.1654 $(M + H)^+$. Calcd for $C_{16}H_{23}FNO_3$ 296.1656. ^{1}H NMR (600 MHz, $CDCl_3$) δ 6.97−6.93 (m, 2 H), 6.88−6.84 (m, 2 H), 4.18−4.03 (m, 2 H), 3.94−3.73 (m, 1 H), 3.46−3.32 (m, 2 H), 2.07−1.81 (m, 4 H), 1.47 (s, 9 H). TLC (UV_{254}) R_f = 0.51 (2:1 hexanes/ethyl acetate).

(*S*)-*tert*-Butyl 2-(Pyrimidin-4-yloxymethyl)pyrrolidine-1-carboxylate (9g). To a stirred solution of *N*-*tert*-butoxycarbonyl-L-prolinol (0.81 g, 4 mmol) **8** in dry DCM (10 mL) was added triphenylphosphine (5.24 g, 20 mmol) followed by 4(3*H*)-pyrimidone (0.77 g, 8mmol). The solution was cooled in an ice bath and DIAD (3.24 g, 16 mmol) added dropwise over 10 min. After 48 h, GC-MS indicated complete conversion of **8** and the reaction mixture was poured onto water (30 mL), the organic fraction collected, and the aqueous phase washed with further DCM (2 × 20 mL). The combined organic fractions were washed with 1 M NaOH (2 × 15 mL) and then brine (1 × 15 mL) and dried over Na_2SO_4. Removal of bulk solvent yielded an orange gum and addition of hexanes/diethyl ether (1:1) resulted in formation of a precipitate of triphenylphosphine oxide, which was removed by filtration. Chromatography (ethyl acetate) afforded the desired product as a colorless oil (0.77 g, 69%). HRMS (ESI) = 280.1655 $(M + H)^+$. Calcd for $C_{14}H_{22}N_3O_3$ 280.1656. ^{1}H NMR (600 MHz, $CDCl_3$) δ 8.71 (s, 1 H), 8.39 (d, J = 6 Hz, 1 H), 6,69 (d, J = 6 Hz, 1 H), 4.45−3.91 (m, 3 H), 3.40−3.33 (m, 2 H), 2.00−1.82 (m, 4 H), 1.42 (s, 9 H). TLC (UV_{254}) R_f = 0.49 (ethyl acetate).

(*S*)-*tert*-Butyl 2-(2-Propynyloxymethyl)pyrrolidine-1-carboxylate (9h). To a stirred solution of **8** (0.40 g, 2 mmol) in dry DMF (10 mL) was added potassium hydroxide (0.56 g, 10 mmol), followed by dropwise addition of propargyl bromide (80 wt. % in toluene) (0.48 g, 4 mmol) over 5 min. After 18 h, the reaction mixture was poured onto water (30 mL) and washed with DCM (3 × 15 mL). The combined organic fractions concentrated in vacuo and the liquid remaining taken up in diethyl ether (15 mL) and washed with water (2 × 10 mL) and then brine (1 × 10 mL) and dried over Na_2SO_4. Chromatography (hexanes/ethyl acetate) gave the desired product as a colorless oil (0.32 g, 67%). HRMS (ESI) = 240.1597 $(M + H)^+$. Calcd for $C_{13}H_{22}NO_3$ 240.1594. ^{1}H NMR (600 MHz, $CDCl_3$) δ 4.13 (s, 2 H), 3.96−3.88 (m, 1 H), 3.64 (dd, J = 9 Hz, J = 3.6 Hz, 1 H), 3.49−3.22 (m, 3 H), 2.40 (s, 1 H), 1.94−1.78 (m, 4 H), 1.46 (s, 9 H). TLC (I_2) R_f = 0.67 (1:1 hexanes/ethyl acetate).

(*S*)-5-(2-(4-Fluorophenoxymethyl)-pyrrolidine-1-sulfonyl)isatin (10b). To a stirred solution of **9b** (0.15 g, 0.5 mmol) in dry DCM (4 mL) cooled in an ice bath was added TFA (0.6 mL, 10 mmol). After 1 h, bulk solvent was removed in vacuo and the residue remaining taken up in dry DCM (8 mL) and cooled in an ice bath. Dry triethylamine (1.5 mL) was then added followed by 5-chlorosulfonylisatin[7] (0.16 g, 0.65 mmol) in dry THF (4 mL) and the solution was then stirred. After 19 h, bulk solvent was removed in vacuo and redissolved in DCM (10 mL), washed with water (2 × 10 mL) and then brine (1 × 10 mL) and dried over Na_2SO_4. Chromatography (hexanes/ethyl acetate) gave the desired product as an orange solid (104 mg, 51%); mp: 205−207 °C. HRMS (ESI) = 405.0941 $(M + H)^+$. Calcd for $C_{19}H_{18}FN_2O_5S$ 405.0920. ^{1}H NMR (600 MHz, $CDCl_3$) δ 8.10 (s,1 H), 8.08 (dd, J = 8.4 Hz, J = 1.8 Hz, 1 H), 8.00 (br, 1 H), 7.00 (d, J = 7.8 Hz, 1 H), 6.99−6.95 (m, 2 H), 6.83−6.81 (m, 2 H), 4.17 (dd, J = 9.6 Hz, J = 3.6 Hz, 1 H), 3.98−3.95 (m, 1 H), 3.91 (dd, J = 9 Hz, J = 7.8 Hz, 1 H), 3.54−3.50 (m, 1 H), 3.24−3.19 (m, 1 H), 2.10−1.99 (m, 2 H), 1.87−1.77 (m, 2 H). TLC (UV_{254}) R_f = 0.27 (2:1 ethyl acetate/hexanes). HPLC t_R = 7.83.

(*S*)-1-(4-Fluorobenzyl)-5-(2-(4-fluorophenoxymethyl)-pyrrolidine-1-sulfonyl)isatin (11b). To a stirred solution of **10b** (40 mg, 0.1 mmol) in dry DMF (3 mL) was added potassium carbonate (21 mg, 0.15 mmol) followed by 4-fluorobenzyl bromide (76 mg, 0.4 mmol). After 2 h, TLC indicated complete conversion of **10b** and the solution was poured onto 10% aq NH_4Cl (10 mL) and extracted with DCM (3 × 10 mL). Combined organic fractions concentrated in vacuo and taken up in diethyl ether (10 mL), washed with water (2 × 10 mL) and then brine (1 × 10 mL) and dried over Na_2SO_4. Chromatography (hexanes/ethyl acetate) gave the title compound as an orange gum (34 mg, 66%). HRMS (ESI) = 513.1306 $(M + H)^+$. Calcd for $C_{26}H_{23}F_2N_2O_5S$ 513.1296. ^{1}H NMR (600 MHz, $CDCl_3$) δ 8.04 (d, J = 1.8 Hz, 1 H), 7.97 (dd, J = 8.4 Hz, J = 1.8 Hz, 1 H), 7.33−7.30 (m, 2 H), 7.09−7.05 (m, 2 H), 6.96−6.92 (m, 2 H), 6.86 (d, J = 8.4 Hz, 1 H), 6.81−6.77 (m, 2 H), 4.92 (d, J = 15.6, 1 H), 4.91 (d, J = 15.6, 1 H), 4.14 (dd, J = 9.6 Hz, J = 3.6 Hz, 1 H), 3.95−3.92 (m, 1 H), 3.88 (dd, J = 9.6 Hz, J = 7.2 Hz, 1 H), 3.51−3.47 (m, 1 H), 3.20−3.15 (m, 1 H), 2.06−1.93 (m, 2 H), 1.83−1.73 (m, 2 H). TLC (UV_{254}) R_f = 0.61 (2:1 ethyl acetate/hexanes). HPLC t_R = 12.25 min.

(*S*)-1-(2-Propynyl)-5-(2-phenoxymethyl-pyrrolidine-1-sulfonyl)isatin (12). To a solution of (*S*)-5-(2-phenoxymethyl-pyrrolidine-1-sulfonyl)isatin **10a**[7] (0.39 g, 1mmol) in dry DMF (10 mL) was added potassium carbonate (0.21 g, 1.5 mmol) followed by propargyl bromide (80 wt. % in toluene) (0.14 g, 1.2 mmol). After 2 h, TLC indicated complete conversion of **10a** and the solution was poured onto 10% aq NH_4Cl (20 mL) and washed with DCM (3 × 10 mL). The combined organic fractions were then reduced in vacuo and the residue taken up in diethyl ether (10 mL) and washed with water (2 × 10 mL) and then brine (1 × 10 mL) and dried over Na_2SO_4. Chromatography (hexanes/ethyl acetate) gave the product as an orange gum. Recrystallization from ethyl acetate/hexanes furnished the product as an orange solid (0.28 g, 66%); mp: 90−92 °C. HRMS (ESI) = 425.1185 $(M + H)^+$. Calcd for $C_{22}H_{21}N_2O_5S$ 425.1171. ^{1}H NMR (600 MHz, $CDCl_3$) δ 8.12 (dd, J = 8.4 Hz, J = 1.8 Hz, 1 H), 8.05 (d, J = 1.8 Hz, 1 H), 7.25−7.21 (m, 2 H), 7.16 (d, J = 8.4 Hz, 1 H), 6.96−6.93 (m, 1 H), 6.81 (d, J = 9 Hz, 2 H), 4.56 (dd, J = 18 Hz, J = 2.4 Hz, 1 H), 4.53 (dd, J = 18 Hz, J = 2.4 Hz, 1 H), 4.19 (dd, J = 9.6 Hz, J = 3 Hz, 1 H), 4.07−4.01 (m, 1 H), 3.97 (dd, J = 9.6 Hz, J = 7.2 Hz, 1 H), 3.55−3.51 (m, 1 H), 3.33−3.28 (m, 1 H), 2.36 (t, J = 2.4 Hz, 1 H), 2.09−1.99 (m, 2 H), 1.89−1.75 (m, 2 H). TLC (UV_{254}) R_f = 0.54 (2:1 ethyl acetate/hexanes). HPLC t_R = 9.00 min.

(*S*)-1-((1-(2-Fluoroethyl)-1*H*-[1,2,3]-triazol-4-yl)methyl)-5-(2-phenoxymethyl-pyrrolidine-1-sulfonyl)isatin (14). To a stirred solution of **12** (138 mg, 0.3 mmol) in dry DMF (3 mL) was added

copper sulfate (38 mg, 0.15 mmol) in water (0.2 mL) followed by ascorbic acid (53 mg, 0.3 mmol) in water (0.2 mL) and then 2-fluoroethylazide[14] (33 mg, 0.36 mmol) in dry DMF (1.5 mL) and the mixture left to stir under argon. After 2 h, TLC indicated reaction completion and mixture was poured onto 10% aq NH_4Cl (12 mL) and extracted with DCM (3 × 10 mL) and dried over Na_2SO_4. Chromatography (hexanes/ethyl acetate) afforded an orange solid (26 mg, 51%); mp: 165−167 °C. HRMS (ESI) = 514.1557 $(M + H)^+$. Calcd for $C_{24}H_{25}FN_5O_5S$ 514.1560. ^1H NMR (600 MHz, $CDCl_3$) δ 8.07 (dd, $J = 8.4$ Hz, $J = 1.8$ Hz, 1 H), 8.01 (d, $J = 1.8$ Hz, 1 H), 7.76 (s, 1 H), 7.47 (d, $J = 8.4$ Hz, 1 H), 7.23−7.19 (m, 2 H), 6.92 (t, $J = 7.8$ Hz, 1 H), 6.82 (d, $J = 7.8$ Hz, 2 H), 5.03 (d, $J = 15.6$ Hz, 1 H), 5.02 (d, $J = 15.6$ Hz, 1 H), 4.79 (dt, $J = 46.2$ Hz, $J = 4.8$ Hz, 2 H), 4.66 (dt, $J = 27$ Hz, $J = 4.8$ Hz, 2 H), 4.17 (dd, $J = 9.6$ Hz, $J = 3.6$ Hz, 1 H), 4.00−3.97 (m, 1 H), 3.93 (dd, $J = 9$ Hz, $J = 7.2$ Hz, 1 H), 3.53−3.49 (m, 1 H), 3.27−3.24 (m, 1 H), 2.08−1.97 (m, 2 H), 1.86−1.75 (m, 2 H). TLC (UV_{254}) R_f = 0.56 (ethyl acetate). HPLC t_R = 7.93 min.

Radiochemistry. Under an atmosphere of nitrogen, a buffered solution (sodium phosphate buffer, pH 6.0, 250 mM) of sodium ascorbate (50 μL, 8.7 mg, 43.2 μmol) was added to a Wheaton vial (1 mL) containing an aqueous solution of copper(II) sulfate (50 μL, 1.7 mg pentahydrate, 7.0 μmol). After one min, a solution of alkyne **13** (3.0 mg, 6.5 μmol) in DMF (25 μL) was added followed by distilled [18F]-2-fluoroethylazide (185−740 MBq) in acetonitrile (100 μL). The mixture was left at room temperature for 30 min, water (15 μL) was added and the resulting mixture was purified by preparative radio-HPLC. The isolated HPLC fraction was diluted with water (5 mL) and loaded onto a SepPak C18-light cartridge (Waters) that had been conditioned with ethanol (5 mL) and water (10 mL). The cartridge was subsequently flushed with water (5 mL) and [18F]**15** eluted with ethanol (0.1 mL fractions). The product fraction was diluted with PBS to provide an ethanol content of 10−15% (v/v).

Log P Determination. Calculated Log P values for all compounds were determined using ACD/Chemsketch Laboratories 10.02. For [18F]**15**, lipophilicity was also assessed by measuring the octanol−water partition coefficient using the method of Barthel et al.[29] Briefly, [18F]**15** (~180 μCi in 25 μL ethanol) was diluted to a final volume of 100 μL with water (stock solution). Aliquots of stock solution (10 μL) were added to water (490 μL) and octan-1-ol (Aldrich anhydrous grade) (500 μL). The solutions were then shaken vigorously for 10 min then centrifuged (13201*g*, 20 °C, 30 min). Following centrifugation, portions (200 μL) of the water and octanol layers were *carefully* removed and analyzed on a Cobra II Auto-Gamma counter (Packard Instruments, Meriden, CT) and compared. The octanol−water partition coefficient was obtained by dividing the octanol containing radioactivity by the water containing radioactivity and the $\log_{10}$ of the ratio calculated.

Caspase Enzyme Inhibition Assays. Recombinant human caspases 1, 3, 6, 7, and 8 and their peptide-specific substrates[9] were purchased from Biomol International, UK. Inhibition of the recombinant caspases by nonradioactive isatins was assessed using a fluorometric assay that measures the accumulation of a fluorogenic product, 7-amino-4-methylcoumarin (7-AMC). All assays were performed in 96-well plates at a volume of 200 μL per well. The assays were performed at 37 °C in an appropriate reaction buffer as described below for each caspase. For caspase 1, the buffer comprised of 0.1% CHAPS, 100 mM NaCl, 5 mM 2-mercaptoethanol, 100 mM HEPES (pH 7.4), 2 mM EDTA, 10% sucrose, and 10 μM of the peptide substrate Ac-YVAD-AMC. For caspase 3: 20 mM HEPES (pH 7.4), 10% sucrose, 100 mM NaCl, 0.1% CHAPS, 2 mM EDTA, and 10 μM Ac-DEVD-AMC. For caspase 6: 20 mM HEPES (pH 7.4), 10% sucrose, 100 mM NaCl, 0.1% CHAPS, 2 mM EDTA, and 10 μM Ac-VEID-AMC. For caspase 7: 20 mM HEPES (pH 7.4), 10% sucrose, 5 mM 2-mercaptoethanol, 100 mM NaCl, 0.1% CHAPS, 2 mM EDTA, 10 μM Ac-DEVD-AMC. For caspase 8: 20 mM HEPES (pH 7.4), 10% sucrose, 100 mM NaCl, 0.1% CHAPS, 2 mM EDTA, and 10 μM Ac-IETD-AMC. The buffers contained nonradioactive isatins in DMSO at a final concentration of 500, 50, 5 μM; 500, 50, 5nM; 500, 50, 5pM; the final concentration of DMSO in all wells was 5% of the total volume. Recombinant caspases were used at 0.5 units per assay (~500 pmol substrate converted per h). All reagents except the peptide substrate were preincubated for 10 min. The peptide substrate (final concentration 10 μM) was then added, and the plate was incubated for a further 30 min; 30 min was selected after initial linearity study where reaction was assessed after 10, 30, 60, or 90 min. Respective control wells contained all reaction components without enzyme. The amount of 7-AMC produced was measured on a fluorescence microplate reader (Victor2; Perkin-Elmer Life sciences) at excitation and emission wavelengths of 355 and 460 nm, respectively. The concentration of isatin that inhibits the caspase activity by 50% (EC50) was estimated by nonlinear regression analysis using GraphPad Prism (Version 4.0 for Windows, GraphPad Software, San Diego, CA). All the isatins were analyzed in duplicate; the assays were repeated once.

In Vitro Mouse Liver S9 Metabolism Studies. Liver S9 metabolism studies were performed as previously described.[30] Mouse livers were rapidly excised and kept at 4 °C throughout the experiment. Tissues were weighed and homogenized in an equivalent volume of 50 mM Tris-150 mM KCl-HCl buffer (pH 7.4) using an Ultra-Thurrax homogenizer (IKA, Staufen, Germany). To obtain the S9 fraction, the homogenate was centrifuged (10000*g*) for 30 min to remove nuclei, mitochondria, and cell debris. Protein concentration of the S9 fraction was determined by a commercial BCA protein assay kit (Perbio Science, Cheshire, UK). S9 fractions were stored at −80 °C for up to 6 weeks. Selected unlabeled isatins **4**, **5**, and **6** (10 mM, 10 μL) were incubated with the S9 fraction (33.26 mg/mL, 20 μL) and 0.5 mM nicotinamide adenine dinucleotide phosphate (reduced form) in air for 60 min at 37 °C in 0.1 mM Tris-HCl buffer (pH 7.4) in a total volume of 1 mL. Control incubation samples contained no isatin. The reactions were terminated by addition of ice-cold acetonitrile (2 mL); the samples were then immediately placed on dry ice prior to extraction and HPLC analysis (below).

Western Blot Analysis. RIF-1 cells were incubated for 15 min with the caspase inhibitors Z-VAD-FMK (Biomol International, UK), isatin **15**, and **4**, and subject to apoptosis with CDDP for 48 h. Protein samples were prepared by lysing RIF-1 cells in RIPA buffer (Invitrogen Ltd., Paisley, UK) supplemented with protease and phosphatase inhibitor cocktails (Sigma-Aldrich Company Ltd., Dorset, UK). Equal amounts of protein (30 μg) were denaturated in sample buffer, subjected to SDS-polyacrylamide gel electrophoresis on 4−12% gels (Invitrogen Ltd., Paisley, UK) and transferred to PVDF membranes (GE Healthcare Life Sciences, Buckinghamshire, UK). The membranes were immunoblotted with specific primary antibodies, horseradish peroxidase-conjugated secondary antibodies, and visualized by enhanced chemiluminescence (GE Healthcare Life Sciences, Buckinghamshire, UK). The following antibodies were used: a mouse monoclonal anticleaved PARP (Cell Signaling Technology Inc., Danvers, MA), a mouse monoclonal antialpha-tubulin, and a goat antimouse HRP (Santa Cruz Biotechnology Inc., Santa Cruz, CA).

In Vitro [18F]15 Uptake and Caspase 3 Activation Assays. Cells were plated in triplicate in 12-well plates 2 or 3 days prior to the experiments and treated with CDDP (Sigma, UK) or vehicle (0.1% DMSO) at the indicated concentration and time. On the day of the experiment, ~10 μCi/well of [18F]15 was added and allowed to accumulate into cells for 60 min at 37 °C. Cells were collected, washed, and resuspended in 400 μL of PBS. Then 260 μL of each sample were transferred in counting tubes and fluorine-18 radioactivity was immediately determined using a Packard Cobra II gamma counter (Perkin-Elmer, UK). BCA Protein assay (Pierce, UK) was performed for all samples and data are normalized and expressed as CCPMA/mg of protein.

In Vivo Biodistribution and Metabolism Studies. The radiation-induced murine fibrosarcoma (RIF-1) tumor cells[31] were maintained in RPMI 1640 medium (Invitrogen Ltd., Paisley, UK) supplemented with 10% fetal calf serum (BioWhittaker Europe Ltd., Verviers, Belgium), 2 mM L-glutamine, 100 U/mL penicillin, 100 μg/mL streptomycin, and 0.25 μg/mL fungizone (Gibco, UK) at

37 °C in a humidified incubator with 5% CO_2. All animal work was done by licensed investigators in accordance with the United Kingdom's "Guidance on the Operation of Animals (Scientific Procedures) Act 1986" (HMSO, London, United Kingdom, 1990) and in full compliance with government regulations and guidelines on the welfare of animals in experimental neoplasia.[32] Tumors were established in mice by subcutaneous injection of 5×10^5 cells on the back of male C3H/hej mice (Harlan, Bicester, Oxfordshire, UK). Tumor growth was monitored every two days using electronic calipers, and tumor volume estimated using the equation $(\pi/6) \times L \times W \times D$ (L = length, W = width, and D = depth). Animals were selected for biodistribution studies of [^{18}F]**15** when the tumors reached ~100−150 mm^3; biodistribution of [^{125}I]**4** was done in nontumor-bearing mice. Mice were injected intravenously via the lateral vein with 0.08−0.13 mL of radioactivity (~0.37 MBq of [^{125}I]**4** or 3.7 MBq of [^{18}F]**15**) dissolved in phosphate buffered saline. At selected times after injection (2−60 min), mice were sacrificed by exsanguination via cardiac puncture under general anesthesia (isofluorane inhalation). Aliquots of heparinized blood were rapidly centrifuged (2000*g* for 5 min) to obtain plasma. The radioactivity contained in tissues was determined by gamma-counting on a Cobra II Auto-Gamma counter (Packard Instruments, Meriden, CTA) and expressed as a percentage of injected dose per gram of tissue (%ID/g). A minimum of three mice were used for each time point. All animals were treatment-naïve.

Furthermore we assessed the uptake of [^{18}F]**15** in treated animals. For this, 60 min biodistribution studies were done in RIF-1 tumor-bearing mice as above but following treatment with vehicle (50% DMSO in saline) or 10 mg/kg CDDP in vehicle for 24 h. Tumor tissues were removed, weighed, and counted for [^{18}F] radioactivity. Data were expressed as tumor/ blood ratios.

In vivo metabolism studies were also performed in C3H/hej mice. Nontumor-bearing mice were injected intravenously with 0.37 MBq of [^{125}I]**4** or 7.4 MBq of [^{18}F]**15** and plasma was obtained as above. Plasma, liver, and urine (in the case of [^{18}F]**15**) samples were snap-frozen in liquid nitrogen and kept in preweighed scintillation counting tubes on dry ice prior to analysis.

HPLC Analysis. Immediately prior to extraction, the samples were thawed and placed on ice. For extraction, ice cold acetonitrile (1.5 mL) was added to plasma (0.2 mL); S9 incubation samples (3 mL) containing acetonitrile were also analyzed. Each mixture was centrifuged (15493*g*, 4 °C, 3 min) and the resulting supernatant was evaporated to dryness under vacuum at 40 °C using a rotary evaporator. Liver samples were homogenized with ice cold acetonitrile (1.5 mL) using an IKA Ultra-Turrax T-25 homogenizer prior to centrifugation. The residues were then resuspended in HPLC mobile phase (1.2 mL) and filtered through a Minisart hydrophilic syringe filter (0.2 μm) (Sartorius, Goettingen, Germany). Urine samples were diluted with HPLC mobile phase and filtered as above. The samples (1 mL) were then analyzed by radio-HPLC on an Agilent 1100 series HPLC system (Agilent Technologies, Stockport, UK) equipped with a γ-RAM model 3 gamma-detector (IN/US Systems Inc., Florida) and the Laura software.

The stationary phase comprised of a Waters μBondapak C_{18} reverse-phase column (300 mm × 7.8 mm). For analysis of [^{125}I]**4**, plasma and liver samples were processed as above and analyzed by using a mobile phase comprising of water (0.1% TFA)/propan-1-ol (0.1% TFA) (35:65) running in isocratic mode at a flowrate of 2 mL/min. For assessment of unlabeled **4**, **5**, and **6** after in vitro metabolism, samples were separated using a mobile phase comprising of water (0.1% TFA)/propan-1-ol (0.1% TFA) with a gradient of 2 → 80% organic in 11 min, 80 → 5% organic in 3 min, and then 5% organic for 6 min delivered at a flowrate of 3 mL/min. For analysis of [^{18}F]**15**, plasma, liver, and urine samples were analyzed using a mobile phase comprising of 0.1 M ammonium formate /1.8:1 methanol:acetonitrile with a gradient of 50% organic for 1 min, 50 → 90% organic in 14 min, 90% organic for 3 min, 90 → 50% organic in 2 min, 50% organic for 4 min delivered at a flowrate of 3 mL/min. Furthermore, to assess the fraction of [^{18}F]**15**-derived radioactivity associated with the plasma and liver pellets after extraction versus that remaining in the HPLC injectate, the total volume of HPLC injectate was recorded and an aliquot (0.1 mL) removed for counting. The radioactivity in the 0.1 mL aliquot and the pellet were then analyzed by gamma counting (Packard Instruments).

Acknowledgment. This work was funded by Cancer Research UK programme grant C2536/A5708 and UK Medical Research Council core funding grant U.1200.02.005.00001.01. We thank Dr Harold Toms, Queen Mary and Westfield College, for NMR assistance, and the EPSRC National Mass Spectroscopy Service Centre (Swansea, UK) for carrying out some of the mass spectral analysis.

Supporting Information Available: Experimental and analytical data for compounds **9c**−**9f**, **10c**−**10h**, **11c**−**11 h**, **13**, **15**, and **16**. Further HPLC chromatograms relating to the metabolism studies, tables of purity data, HPLC chromatograms, and ^{1}H NMR spectra for compounds **2**, **4**, **5**, **6**, **11b**−**h**, **13**, **14**, **15**, and **16**. This material is available free of charge via the Internet at http://pubs.acs.org.

References

(1) Okada, H.; Mak, T. W. Pathways of apoptotic and non-apoptotic cell death in tumor cells. *Nat. Rev. Cancer* **2004**, *4*, 592–603.
(2) Reed, J. C. Apoptosis-Based Therapies. *Nat. Rev. Drug Discovery* **2002**, *1*, 111–121.
(3) Denault, J.-B.; Salvesen, G. S. Caspases: Keys in the Ignition of Cell Death. *Chem. Rev.* **2002**, *102*, 4489–4499.
(4) Degterev, A.; Boyce, M.; Yuan, J. A decade of caspases. *Oncogene* **2003**, *22*, 8543–8567.
(5) Nicholson, D. W.; Thornberry, N. A. Caspases: killer proteases. *Trends Biochem. Sci.* **1997**, *22*, 299–306.
(6) Earnshaw, W. C.; Martins, L. M.; Kaufmann, S. C. Mammalian Caspases: Structure, Activation, Substrates, and Functions During Apoptosis. *Annu. Rev. Biochem.* **1999**, *68*, 383–424.
(7) Lee, D.; Long, S. A.; Murray, J. H.; Adams, J. L.; Nuttall, M. E.; Nadeau, D. P.; Kikly, K.; Winkler, J. D.; Sung, C.; Ryan, M. D.; Levy, M. A.; Keller, P. M.; DeWolf, W. E. Potent and Selective Nonpeptide Inhibitors of Caspases 3 and 7. *J. Med. Chem.* **2001**, *44*, 2015–2026.
(8) Chu, W.; Zhang, J.; Zeng, C.; Rothfuss, J.; Tu, Z.; Chu, Y.; Reichert, D. E.; Welch, M. J.; Mach, R. H. *N*-Benzylisatin sulfonamide analogues as potent caspase-3 inhibitors: synthesis, in vitro activity, and molecular modeling studies. *J. Med. Chem.* **2005**, *48*, 7637–7647.
(9) Kopka, K.; Faust, A.; Keul, P.; Wagner, S.; Breyholz, H.; Höltke, C.; Schober, O.; Schäfers, M.; Levkau, B. 5-Pyrrolidinylsulfonyl Isatins as a Potential Tool for the Molecular Imaging of Caspases in Apoptosis. *J. Med. Chem.* **2006**, *49*, 6704–6715.
(10) Zhou, D.; Chu, W.; Rothfuss, J.; Zeng, C.; Xu, J.; Jones, L.; Welch, M. J.; Mach, R. H. Synthesis, radiolabelling, and in vivo evaluation of an 18F-labeled isatin analog for imaging caspase-3 activation in apoptosis. *Bioorg. Med. Chem. Lett.* **2006**, *16*, 5041–5046.
(11) Kuijpers, B. H. M.; Groothuys, S.; Soede, A.; Laverman, P.; Boerman, O. C.; van Delft, F. L.; Rutjes, F. P. J. T. Preparation and Evaluation of Glycosylated Arginine-Glycine-Aspartate (RGD) Derivatives for Integrin Targeting. *Bioconjugate Chem.* **2007**, *18*, 1847–1854.
(12) Li, Z.; Wu, Z.; Chen, K.; Chin, F. T.; Chen, X. Click Chemistry for 18F-Labeling of RGD Peptides and microPET Imaging of Tumor Integrin $\alpha_v\beta_3$ expression. *Bioconjugate Chem.* **2007**, *18*, 1987–1994.
(13) Marik, J.; Sutcliffe, J. L. Click for PET: rapid preparation of [^{18}F]fluoropeptides using Cu^1 catalyzed 1,3-dipolar cycloaddition. *Tetrahedron Lett.* **2006**, *47*, 6681–6684.
(14) Glaser, M.; Årstad, E. "Click Labeling" with 2-[^{18}F]Fluoroethylazide for Positron Emission Tomography. *Bioconjugate Chem.* **2007**, *18*, 989–993.
(15) Wipf, P.; Jung, J.-K.; Rodríguez, S.; Lazo, J. S. Synthesis and biological evaluation of deoxypreussomerin A and palmarumycin CP_1 and related napthoquinone spiroketals. *Tetrahedron* **2001**, *57*, 283–296.
(16) Park, B. K.; Kitteringham, N. R.; O'Neill, P. M. Metabolism of fluorine-containing drugs. *Annu. Rev. Pharmacol. Toxicol.* **2001**, *41*, 443–470.
(17) Rietjens, I. M. C. M.; Soffers, A. E. M. F.; Veeger, C.; Vervoort, J. Regioselectivity of Cytochrome P-450 Catalyzed Hydroxylation of Fluorobenzenes Predicted by Calculated Frontier Orbital Substrate Characteristics. *Biochemistry* **1993**, *32*, 4801–4812.
(18) Lahorte, C. M. M.; Vanderheyden, J.-L.; Steinmetz, N.; Van de Wiele, C.; Dierckx, R. A.; Slegers, G. Apoptosis-detecting radioligands: current state of the art and future perspectives. *Eur. J. Nucl. Med. Mol. Imaging* **2004**, *31*, 887–919.

(19) Boersma, H. H.; Kietselaer, B. L. J. H.; Stolk, L. M. L.; Bennaghmouch, A.; Hofstra, L.; Narula, J.; Heidendal, G. A. K.; Reutelingsperger, C. P. M. Past, Present, and Future of Annexin A5: From Protein Discovery to Clinical Applications. *J. Nucl. Med.* **2005**, *46*, 2035–2050.

(20) Aloya, R.; Shirvan, A.; Grimberg, H.; Reshef, A.; Levin, G.; Kidron, D.; Cohen, A.; Ziv, I. Molecular imaging of cell death in vivo by a novel small molecule probe. *Apoptosis* **2006**, *11*, 2089–2101.

(21) Damianovich, M.; Ziv, I.; Heyman, S. N.; Rosen, S.; Shina, A.; Kidron, D.; Aloya, T.; Grimberg, H.; Levin, G.; Reshef, A.; Bentolila, A.; Cohen, A.; Shirvan, A. *ApoSense*: a novel technology for functional molecular imaging of cell death in models of acute renal tubular necrosis. *Eur. J. Nucl. Med. Mol. Imaging* **2006**, *33*, 281–291.

(22) Ziv, I.; Shirvan, A. Perturbed membrane-binding compounds and methods of using the same. WO 2005/067388, 2005.

(23) Thornberry, N. A.; Rano, T. A.; Peterson, E. P.; Rasper, D. M.; Timkey, T.; Garcia-Calvo, M.; Houtzager, V. M.; Nordstrom, P. A.; Roy, S.; Vaillancourt, J. P.; Chapman, K. T.; Nicholson, D. W. A Combinatorial Approach Defines Specifities of Members of the Caspase Family and Granzyme B. *J. Biol. Chem.* **1997**, *272* (29), 17907–17911.

(24) Bauer, C.; Bauder-Wuest, U.; Mier, W.; Haberkorn, U.; Eisenhut, M. 131I-Labeled Peptides as Caspase Substrates for Apoptosis Imaging. *J. Nucl. Med.* **2005**, *46* (6), 1066–1074.

(25) Aulabaugh, A.; Kapoor, B.; Huang, X.; Dollings, P.; Hum, W.; Banker, A.; Wood, A.; Ellestad, G. Biochemical and Biophysical Characterization of Inhibitor Binding to Caspase-3 Reveals Induced Asymmetry. *Biochemistry* **2007**, *46*, 9462–9471.

(26) Lee, D.; Long, S. A.; Adams, J. L.; Chan, G.; Vaidya, K. S.; Francis, T. A.; Kikly, K.; Winkler, J. D.; Sung, C.; Debouck, C.; Richardson, S.; Levy, M. A.; DeWolf, W. E.; Keller, P. M.; Tomaszek, T.; Head, M. S.; Ryan, M. D.; Haltiwanger, R. C.; Liang, P.; Janson, C. A.; McDevitt, P. J.; Johanson, K.; Concha, N. O.; Chan, W.; Abdel-Meguid, S. S.; Badger, A. M.; Lark, M. W.; Nadeau, D. P.; Suva, L. J.; Gowen, M.; Nuttall, M. E. Potent and Selective Nonpeptide Inhibitors of Caspases 3 and 7 Inhibit Apoptosis and Maintain Cell Functionality. *J. Biol. Chem.* **2000**, *275*, 16007–16014.

(27) Leist, R.; Frey, J. A.; Ottiger, P.; Frey, H.; Leutwyler, S.; Bachorz, R. A.; Klopper, W. Nucleobase−Fluorobenzene Interactions: Hydrogen Bonding Wins over π Stacking. *Angew. Chem., Int. Ed.* **2007**, *46*, 7449–7452.

(28) Aboagye, E. O.; Bhujwalla, Z. M.; Shungu, D. C.; Glickson, J. D. Detection of Tumor Response to Chemotherapy by 1H Nuclear Magnetic Resonance Spectroscopy: Effect of 5-Fluorouracil on Lactate Levels in Radiation-Induced Fibrosarcoma 1 Tumors. *Cancer Res.* **1998**, *58*, 1068–1073.

(29) Barthel, H.; Wilson, H.; Collingridge, D. R.; Brown, G.; Osman, S.; Luthra, S. K.; Brady, F.; Workman, P.; Price, P. M.; Aboagye, E. O. In vivo evaluation of [^{18}F]fluoroetanidazole as a new marker for imaging tumour hypoxia with positron emmission tomography. *Br. J. Cancer* **2004**, *90*, 2232–2242.

(30) Aboagye, E. O.; Lewis, A. D.; Tracy, M.; Workman, P. Bioreductive Metabolism of the Novel Fluorinated 2-Nitroimidazole Hypoxia Probe *N*-2-Hydroxy-3,3,3-trifluoropropyl0-2-(2-nitroimidazolyl) Acetamide (SR-4554). *Biochem. Phamacol.* **1997**, *54*, 1217–1224.

(31) Twentyman, P. R.; Brown, J. M.; Gray, J. W.; Franko, A. J.; Scoles, M. A.; Kallman, R. F. A New Mouse Tumor Model System (RIF-1) for Comparison of End-Point Studies. *J. Nat. Cancer Inst* **1980**, *64*, 595–604.

(32) Workman, P.; Twentyman, P.; Balkwill, F.; Balmain, A.; Chaplin, D.; Double, J.; Embleton, J.; Newell, D.; Raymond, R.; Stables, J.; Stephens, T. C.; Wallace, J. United Kingdom Coordinating Committee on Cancer Research (UKCCCR) Guidelines for the welfare of animals in experimental neoplasia. *Br. J. Cancer* **1998**, *77*, 1–10.

JM801107U